Dose distributions in adult and child head phantoms for panoramic and cone beam computed tomography imaging of the temporomandibular joint

Durer Iskanderani, BDS, MDSc,[a,b] Mats Nilsson, PhD,[a,c] Per Alstergren, DDS, PhD,[d] and Kristina Hellén-Halme, DDS, PhD[a]

Objectives. The aim of this study was to map and compare the distributions of absorbed doses with Gafchromic film for panoramic radiography and cone beam computed tomography (CBCT) examinations of the temporomandibular joint (TMJ) by using adult and child phantoms.

Study Design. Gafchromic films were placed at 5 selected levels of anthropomorphic head phantoms of an adult and a child. Clinical protocols for panoramic and CBCT imaging of the TMJ were used for three 2-dimensional or 3-dimensional dental x-ray units. Mean absorbed doses in a set of radiosensitive tissues within the oral and maxillofacial regions were estimated.

Results. The absorbed doses varied considerably among and within radiosensitive tissues. The bone surface and the salivary glands received the highest absorbed doses compared with other tissues, in both panoramic and CBCT examinations of the TMJ. The radiation burden to the adult phantom was generally higher than that to the child phantom. Small right and left fields of view were associated with lower amounts of radiation, in contrast to a single larger field of view.

Conclusions. The absorbed dose within all radiosensitive tissues varied considerably in relation to examination type, x-ray unit, clinical settings, and patient age. The mean doses were smaller when using 2 (bilateral) 4 × 4 cm volumes than with use of one 14 × 5 cm volume. (Oral Surg Oral Med Oral Pathol Oral Radiol 2020;130:200−208)

Radiography is a valuable and useful diagnostic tool that is widely used in dentistry. For verifying clinical findings and improving the quality of the diagnostic decision as well as the treatment plan, more and more radiographic examinations are being performed. As a result, total patient radiation dose has increased over time in combination with the presence of radiosensitive structures in the oral and maxillofacial region, raising concerns about the total delivered dose. This is potentially more risky for young patients whose developing tissues are more radiosensitive.[1] Thus, radiographic examinations should hold radiation doses to a minimum level that still delivers the required diagnostic information, according to the ALADA (As Low As Diagnostically Acceptable) principle.[2]

In general dental practice, panoramic imaging often helps map the maxillofacial region and rule out odontogenic sources of disease or gross osseous alterations.[3] However, the technique has poor reliability among observers and low sensitivity; that is, it underestimates the radiologic findings of disease. For this reason, it has limited use in investigating temporomandibular joint (TMJ)−related osseous changes[4,5] and is not included in the diagnostic criteria for temporomandibular disorder (TMD).[4] Three-dimensional TMJ imaging has been associated with better appreciation of TMJ anatomy and function.[3] Thus, additional cone beam computed tomography (CBCT) imaging is recommended when detailed diagnostic information is required, further radiographic imaging is needed, or standard treatment has failed. Several previous studies have indicated the important contribution of CBCT imaging to TMJ diagnosis and treatment planning because of its high diagnostic accuracy and the relatively low radiation dose compared with other 3-dimensional (3-D) imaging techniques, such as multidetector computed tomography (CT).[6-8] CBCT units, which offer varying spatial resolutions and radiation doses, provide clinicians with a variety of protocols and fields of view (FOVs) for imaging the TMJ.

The literature describes various dosimetric methods for evaluating radiation dose distributions. Gafchromic film dosimetry, in particular, is one of the more common methods for providing dose verification and for measuring dose maps with high spatial resolution, low

Statement of Clinical Relevance

Accurate measurement of the absorbed dose in the small radiation fields in dental radiology is challenging. The use of Gafchromic film has shown promising outcomes for mapping absorbed dose distributions, permitting dose comparisons between adults and children, and among different protocols.

[a]Department of Oral and Maxillofacial Radiology, Faculty of Odontology, Malmö University, Malmö, Sweden.
[b]Department of Oral and Maxillofacial Radiology, Faculty of Dentistry, King Abdulaziz University, Jeddah, Saudi Arabia.
[c]Department of Medical Radiation Physics, Skåne University Hospital, Malmö, Sweden.
[d]Department of Orofacial Pain and Jaw Function, Faculty of Odontology, Malmö University, Malmö, Sweden.
Received for publication Jul 17, 2019; returned for revision Jan 4, 2020; accepted for publication Jan 11, 2020.

2212-4403/$-see front matter
https://doi.org/10.1016/j.oooo.2020.01.003

energy dependence, and adequate accuracy.[9-11] Gafchromic film is a self-developing film and has a radiosensitive layer that contains a crystalline diacetylene monomer, which, when irradiated, polymerizes and darkens.[12] The amount of darkening is related to the absorbed dose.[12]

Several studies have measured doses absorbed during radiographic TMJ examinations by using thermoluminescent dosimeters (TLDs).[13-17] In organ dose measurements, TLDs are associated with limited spatial resolution; this is a disadvantage in situations with steep dose gradients.[18] Gafchromic film has been suggested as a more feasible tool for radiation measurements,[12,19,20] but only 1 report has described the use of Gafchromic film in TMJ dosimetry.[20] The aim of this study was to map and compare the absorbed dose distributions with Gafchromic films in panoramic radiography and CBCT examinations of the TMJ by using adult and child phantoms.

MATERIALS AND METHODS

Imaging units

Absorbed dose distributions were measured by using 3 dental x-ray units from the same manufacturer (J. Morita Corp., Kyoto, Japan): Veraviewepocs 3-D F40, Veraview X800, and 3-D Accuitomo 170. Panoramic exposures were made with the Veraviewepocs 3-D F40 and Veraview X800 units using both the adult and child protocols with 220-degree rotation. CBCT volumes were centered on the TMJs bilaterally and made with the Veraviewepocs 3-D F40 and Veraview X800 units using both the adult and child protocols. The Veraviewepocs 3-D F40 was used at 180-degree (half) rotation (this unit is limited to 180-degree rotation), and exposures were made with the Veraview X800 unit at 360-degree (full) rotation and 180-degree (half) rotation with both units using a 4 × 4 cm FOV. The 3-D Accuitomo 170 used adult and child protocols, each with full- and half-rotations, at 4 × 4 cm and 14 × 5 cm FOVs. All instrument settings were those commonly used in the clinic, according to the manufacturer's recommendation (Table I).

Phantoms and Gafchromic films

Two phantoms were used in dose distribution measurements: the head section of an adult anthropomorphic RANDO phantom, which was 175 cm in height and 73.5 kg in weight (The Phantom Laboratory, Salem, NY); and the head of a CIRS anthropomorphic phantom of an average 10-year-old child, 140 cm in height and 32 kg in weight (Computerized Imaging Reference Systems, Norfolk, VA). Both phantoms were cross-sectional in design, with 25-mm-thick sections, and consisted of a human skeleton (RANDO) or bone-equivalent material (CIRS) embedded in soft tissue−equivalent materials. For each adult phantom slice, the boundaries of the organs of interest were delineated by using an anatomy atlas.[21] At the time of this study, the literature had no cross-sectional anatomy atlas that could be consulted for a 10-year-old child, so an oral radiologist studied a number of anonymized CT examinations of 10-year-old children in the hospital image archive to estimate organ shape and location. These findings were correlated with the corresponding structures in the adult anatomy atlas. In general, the sites were similar, with minor differences among the slices.

Table I. Exposure parameters of the three dental x-ray units used for panoramic and CBCT examinations

Protocol	*Unit*	*kV*	*mAs*	*Rotation*	*FOV*
1. Panoramic adult	Veraviewepocs 3-D F40	70	74	220	N/A
2. Panoramic child	Veraviewepocs 3-D F40	64	65	220	N/A
3. Panoramic adult	Veraview X800	75	119	220	N/A
4. Panoramic child	Veraview X800	75	104	220	N/A
5. CBCT, TMJ B, adult	Veraviewepocs 3-D F40	90	47	180	4 × 4
6. CBCT, TMJ B, child	Veraviewepocs 3-D F40	90	47	180	4 × 4
7. CBCT, TMJ B, adult	Veraview X800	100	107	360	4 × 4
8. CBCT, TMJ B, adult	Veraview X800	100	56	180	4 × 4
9. CBCT, TMJ B, child	Veraview X800	100	90	360	4 × 4
10. CBCT, TMJ B, child	Veraview X800	100	47	180	4 × 4
11. CBCT, TMJ B, adult	3-D Accuitomo 170	90	105	360	4 × 4
12. CBCT, TMJ B, adult	3-D Accuitomo 170	90	54	180	4 × 4
13. CBCT, TMJ B, child	3-D Accuitomo 170	90	105	360	4 × 4
14. CBCT, TMJ B, child	3-D Accuitomo 170	90	54	180	4 × 4
15. CBCT, TMJ B, adult	3-D Accuitomo 170	90	105	360	14 × 5
16. CBCT, TMJ B, adult	3-D Accuitomo 170	90	54	180	14 × 5
17. CBCT, TMJ B, child	3-D Accuitomo 170	90	105	360	14 × 5
18. CBCT, TMJ B, child	3-D Accuitomo 170	90	54	180	14 × 5

B, bilateral; *CBCT,* cone beam computed tomography; *FOV,* field of view; *kV,* kilovolt; mAs, milliampere-seconds; *N/A,* not applicable; *TMJ,* temporomandibular joint.

Gafchromic XR-QA2 film (ISP Corp., Wayne, NJ) was used as the dose measurement tool. Because the Gafchromic film response to absorbed dose is nonlinear, it was calibrated against a Radcal 10 × 6-6 ionization chamber (Radcal Corporation, Monrovia, CA).[12] The film was exposed to 8 doses of radiation between 2000 and 110,000 μGy; 1 nonirradiated film was used for calculating the background value. In a previous study,[11] the film was calibrated for kilovolt (kV) settings from 60 to 120 kV by using the same ionization chamber (which has a flat energy response in this interval). It was found that the calibration curves coincided. Therefore, the same calibration curve could be used for all exposure settings. All films were scanned into 24-bit RGB images (8-bit per channel) on an Epson Perfection 4990 Photo flatbed scanner (Seiko Epson Corp., Nagano, Japan) with a consistent orientation by using a template for the shape of each phantom level.

The images were then converted into 8-bit gray scale and analyzed with ImageJ software (National Institutes of Health, Bethesda, MD) to calculate net pixel values (pixel value in the exposed image minus the mean pixel value in the background film) to plot a dose−response calibration curve (Figure 1). Before applying the dose calibration equation to the net pixel value data, these were converted to 32-bit floating point data to avoid truncation errors.

Radiation dose measurements

Scout images of the phantoms were made to ensure correct and reproducible positioning within the selected FOV, with the sectional planes parallel to the floor. Gafchromic films were loaded into 5 levels of the phantoms. For panoramic examination, 1 film was centered at the occlusal level, and 2 films were positioned superiorly and 2 inferiorly. For the TMJ examination, 1 film was centered on the TMJ region, and 2 films were positioned superiorly and 2 inferiorly. For each examination protocol, the central beam of all radiation fields was deliberately placed 1 cm away from the central level where a film was placed, thus avoiding irradiating the film with a parallel beam (Figure 2). Multiple exposures were made to obtain a dose that was within the dynamic range of the Gafchromic films (see Table I). After reading the image into the ImageJ program and subtracting the background value, we converted the net pixel value matrix to absorbed dose by using the dose−response curve. The absorbed dose matrix was then divided by the number of exposures, which provided an absorbed dose matrix for 1 exposure, that is, the clinical situation. Figure 3 illustrates the steep dose gradients in 1 panoramic and 2 CBCT examinations.

The mean doses absorbed by the radiosensitive structures within the oral and maxillofacial region (brain, eyes, salivary glands, oral mucosa, and bone surface) were estimated by overlapping the corresponding regions of interest on the dose distribution matrices and calculating the mean absorbed dose inside each region of interest. This was repeated for all film sheets from both phantoms. For large structures lying in multiple phantom levels, the mean values were calculated by the mean of the mean values in which the structure was present.

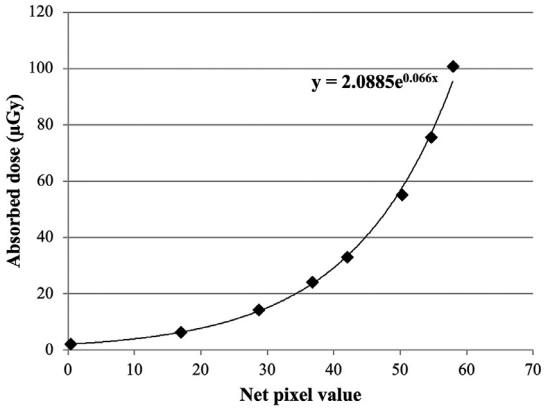

Fig. 1. Dose response calibration curve for Gafchromic XR-QA2 film, Lot # 07271701 (ISP Corp., Wayne, NJ).

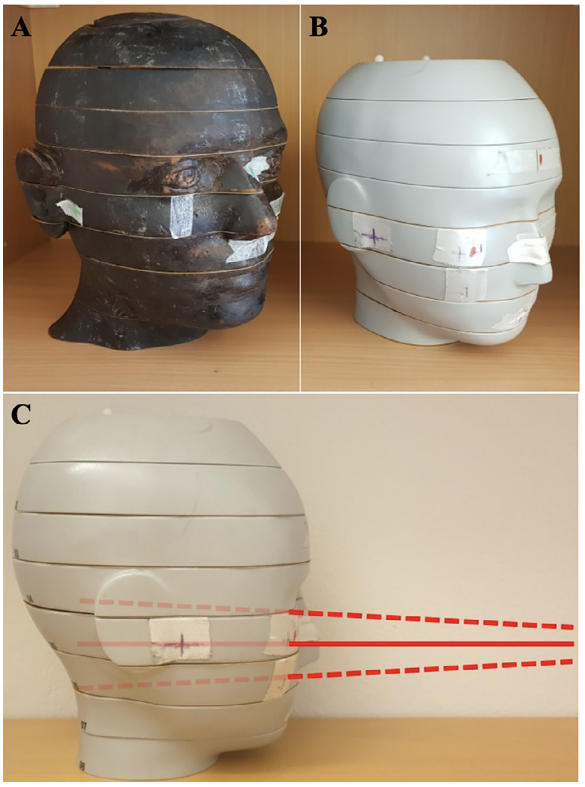

Fig. 2. Phantoms loaded with Gafchromic films on 5 levels. **A**, Adult phantom, for temporomandibular joint examination. **B**, Child phantom, for panoramic examination, as indicated by the numbers. **C**, Child phantom with the central x-ray beam placed 1 cm away from the central level where a film was placed, thus avoiding irradiating the film with a parallel beam.

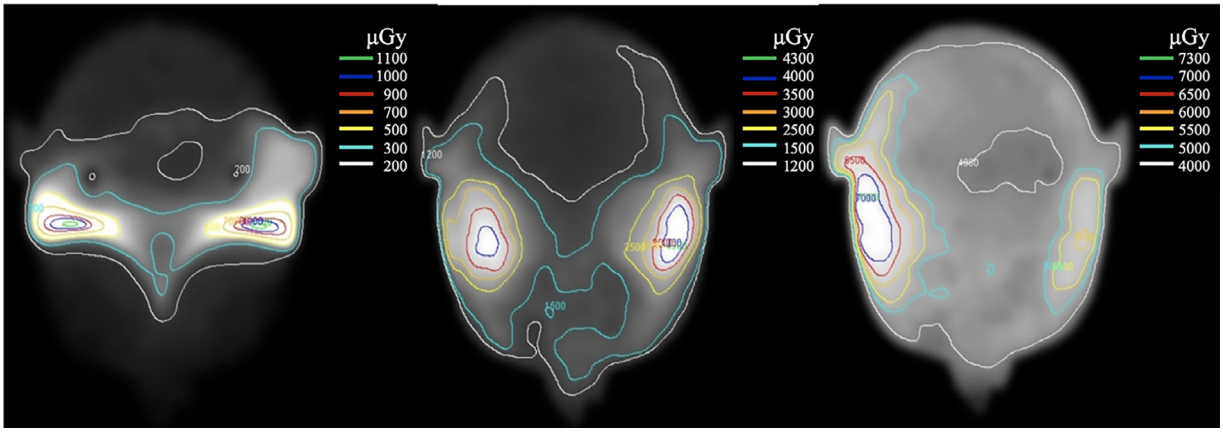

Fig. 3. Absorbed dose distributions are given as isodose lines in microgray for an adult phantom *(left to right)*: A panoramic examination and temporomandibular joint (TMJ) examinations, using two 4 × 4 cm and one 14 × 5 cm cone beam computed tomography (CBCT) volumes.

Deriving the absorbed dose to bone surface needs special attention. The higher atomic number for bone will result in a higher absorbed dose value at a point than it would have been for soft tissue. This can be accounted for by multiplying the measured dose value with the ratio of the mass energy absorption coefficients, μ_{en}/ρ, for bone and soft tissue, respectively.[22] As this ratio is strongly dependent on photon energy, it has to be evaluated for the different situations at hand. The mean photon energies for the x-ray spectra using kV (see Table I) and total filtration (Table II) were calculated,[23] representing the x-ray spectrum impinging on the phantom. In addition, the mean photon energies after penetration of 100 mm of soft tissue were calculated. The mean of these 2 values was used for estimating the ratio of the mass energy absorption coefficients, which were retrieved from Evans.[24] For the x-ray spectra in question, the ratio values varied from 3.0 to 4.1.

The values obtained were comparable for the different x-ray units, phantoms, and protocols. For convenience, the values in Tables III through VI were normalized to one of the protocols, and this allowed for calculation of relative radiation burden percentages.

Table II. Parameters affecting the depth dose characteristics for the 3 CBCT units used in this study

Unit	*Isocenter distance (mm)*	*Total filtration (mm Al)*	*kV*
Veraviewepocs 3-D F40	340	9.5	90
Veraview X800	400	11	100
3-D Accuitomo 170	540	4.7	90

CBCT, cone beam computed tomography; *kV,* kilovolt.

Measurement uncertainty

The overall error of the absorbed dose estimation in 1 single pixel, ε, is caused by:

1. Uncertainty of the calibration of the ionization chamber. For an instrument of this type it is typically in the order of ± 10%.
2. Uncertainty of determining the net pixel value in the 8-bit images for the dose calibration curve. As the pixel values in a uniformly irradiated film follow a normal distribution, this error (standard error of measurement) is around ± 1.5%.
3. Uncertainty of the curve fitting to the dose points (see Figure 1). This is around ± 8%.
4. Uncertainty of determining the pixel value as a result of truncation errors in the point where the dose is calculated. This error is around ± 2%.

Table III. Mean absorbed doses for the organs of interest in the panoramic examinations of an adult and a child phantom with two 2-D/3-D combined dental imaging units (J. Morita Corp., Kyoto, Japan)

Organ	*Mean absorbed organ doses (µGy)*			
	Veraviewepocs 3-D F40		*Veraview X800*	
	Adult	*Child*	*Adult*	*Child*
Brain	150	80	210	150
Eyes	100	70	140	110
Salivary glands	700	660	850	940
Oral mucosa	250	190	260	270
Bone surface	1440	980	1670	1480
Relative radiation burden %	100*	67	114	104

*Normalization value for panoramic examinations.
µ*Gy,* microgray.

Accordingly, the overall uncertainty of the absorbed dose estimation *in 1 single point*, ε, can be estimated to $\pm$ 13%. However, all results presented in this paper are *mean* doses to different organs and tissues. The mean doses are calculated from thousands of measurement points. Therefore, the overall error of the mean values given in Tables III through VI is $\frac{\varepsilon}{\sqrt{n}}$, where n is the total number of pixels used to calculate the mean absorbed dose. The uncertainties of the mean values are, therefore, very small. This applies even more to the integration of the radiation burden, which is carried out over millions of measurement points.

RESULTS

Table III shows the mean absorbed dose for each organ of interest in panoramic examinations of the adult and child phantoms with the 2 dental x-ray units that could produce panoramic images. Tables IV and V present mean absorbed doses in CBCT examinations of the same organs of interest in the adult and child phantoms using full (see Table IV) and half (see Table V) rotations with 2 and 3 dental x-ray units, respectively. In all examinations, the highest absorbed doses occurred in the bone surface and the salivary glands for both the panoramic and the CBCT examinations. The other organs and tissues received 270 μGy or less during the panoramic examination and 1530 μGy or less in a small FOV of the full- and half-rotation CBCT scans. The radiation burden to the adult phantom was generally higher than that for the child phantom.

For both panoramic and full-rotation CBCT examinations, Veraview X800 delivered the highest radiation burden compared with the other units (see Tables III and IV). In contrast, 3-D Accuitomo 170 delivered the lowest radiation burden during the CBCT examinations, at both full- and half-rotation angles (see Tables IV and V). The Veraviewepocs 3-D F40 unit showed the highest radiation burden of the 3 units for half-rotation scans (see Table V).

Table VI presents the mean organ dose for the adult and child phantoms at different FOVs for CBCT imaging with the Accuitomo 170 unit. The mean organ dose was lower in 2 small FOVs than in 1 large FOV with only a few exceptions. When comparing these 2 situations, we also found a 27% lower relative radiation burden in the bilateral 4 × 4 FOVs compared with one l4 × 5 FOV in a 360-degree rotation for both phantoms, whereas 16% and 22% reductions were found with a 180-degree rotation for the adult and child phantoms, respectively (Figure 4).

Table IV. Mean absorbed doses for the organs of interest in full-rotation CBCT examinations of an adult phantom and a child phantom with 2 dental imaging units (J. Morita Corp., Kyoto, Japan)

Organ	*Mean absorbed organ doses (μGy)*			
	Veraview X800		*3-D Accuitomo 170*	
	Adult	*Child*	*Adult*	*Child*
Brain	950	680	680	570
Eyes	570	1530	870	1210
Salivary glands	3510	3070	1960	2210
Oral mucosa	610	480	430	380
Bone surface	5880	6030	4390	5150
Relative radiation burden %	100*	94	78	73

*Normalization value for CBCT examinations: full-rotation. *CBCT,* cone beam computed tomography; *μGy,* microgray.

DISCUSSION

We chose not to report our results as effective dose. The reason for this is that effective dose is often—and increasingly—not used for its actual purpose.[25-27] The medical community must use the effective dose concept wisely, realizing that an effective dose *estimate* represents a generic estimate of risk from a given procedure to a generic model of the human body. In no way does it represent risk to any one individual. Effective dose should not be used for epidemiologic studies or the estimation of population risks because of the inherent uncertainty and oversimplification involved.[27] This is especially true for children, in our case the phantom for a 10-year-old child. In such a situation, effective dose is not even defined because of lack of data for estimating weighting factors.

The International Commission on Radiologic Protection is aware of and concerned about the widespread misuse of the concept of effective dose and is presently investigating if other quantities can be used or developed as a replacement. Ongoing research aims at introducing alternative ways of estimating radiation risk; for instance, from the use of dose area product measurements together with conversion factors that depend on which body part is irradiated. Dose area product measurements give readings that are proportional to the energy imparted to a certain region of the body. This is why we used the term "radiation burden" in the paper because it also is proportional to the energy imparted.

One attractive method for comparing the radiation burden to the patient in relation to different x-ray units, protocols, and patient ages would have been to use the concept of energy imparted. The definition of energy imparted (ε) to matter in a given volume is the sum of all energy deposits in the volume; thus, $\epsilon = \sum_i \epsilon_i$, where the summation is performed over all energy deposits, ε_i, in that volume. However, we did not have absorbed dose values over the whole volume, only for 5 slices in that volume. By integrating the absorbed dose values in the 5 slices, we would get a useful quantity that represents the "radiation burden" to the patient and which also would be roughly proportional to the energy imparted.

Table V. Mean absorbed doses for the organs of interest in half-rotation CBCT examinations of an adult phantom and a child phantom with 3 dental imaging units (J. Morita Corp., Kyoto, Japan)

Organ	*Mean absorbed organ doses (μGy)*					
	Veraviewepocs 3-D F40		*Veraview X800*		*3-D Accuitomo 170*	
	Adult	*Child*	*Adult*	*Child*	*Adult*	*Child*
Brain	760	560	680	520	480	410
Eyes	350	340	250	370	240	420
Salivary glands	2270	1900	1740	1810	1180	1300
Oral mucosa	320	240	340	250	200	190
Bone surface	3960	3330	3390	3090	2560	2660
Relative radiation burden %	100*	81	82	78	61	60

*Normalization values for CBCT examinations: half-rotation.
CBCT, cone beam computed tomography; *μGy,* microgray.

Table VI. Mean absorbed doses for the organs of interest for adult phantoms and child phantoms when comparing different fields of view for cone beam computed tomography imaging with the 3-D Accuitomo 170 unit (J. Morita Corp., Kyoto, Japan)

Organ	*Mean organ doses (μGy)*							
	Adult phantom				*Child phantom*			
	360-degree rotation		*180-degree rotation*		*360-degree rotation*		*180-degree rotation*	
FOV	*2(4 × 4)*	*14 × 5*	*2(4 × 4)*	*14 × 5*	*2(4 × 4)*	*14 × 5*	*2(4 × 4)*	*14 × 5*
Brain	1360	2220	950	1460	1150	1590	810	1100
Eyes	1740	2290	480	340	2430	4650	850	870
Salivary glands	3930	4400	2370	1810	4420	4630	2610	2440
Oral mucosa	870	1530	400	580	760	1390	390	530
Bone surface	8820	11160	5110	4930	10290	12490	5290	6080
Relative radiation burden %	100*	138	54	65	94	128	53	68

*Normalization value for comparison of 2(4 × 4) with 14 × 5 FOVs.
FOV, field of view.

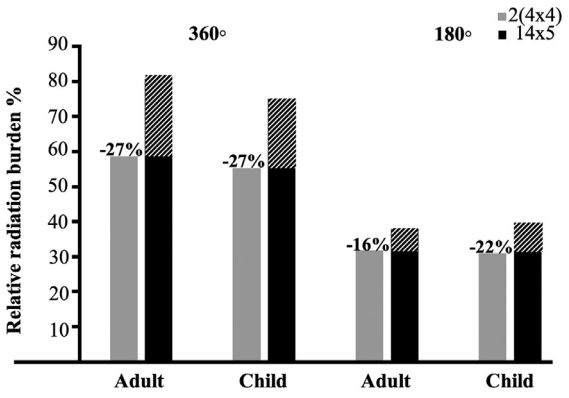

Fig. 4. The percentage of relative radiation burden for adult and child phantoms when comparing different fields of view (FOVs) for cone beam computed tomography (CBCT) imaging (Accuitomo 170, J. Morita Corp., Kyoto, Japan).

In this investigation, we measured radiation burden associated with various examinations by using a variety of imaging techniques, x-ray units, examination settings, FOVs, and phantoms. Because the main purpose of panoramic radiography during TMJ assessment is to rule out odontogenic causes, the standard panoramic radiography mode was included. In panoramic imaging, the Veraviewepocs 3-D F40 unit produced a lower radiation burden compared with the Veraview X800 unit. The most likely reason was that the kilovoltage and milliamperage values were significantly higher for Veraview X800. The higher filtration of Veraview X800 obviously did not fully compensate for this.

Generally, all studied tissues were exposed to considerably more radiation in CBCT examinations compared with panoramic examinations, and this finding is consistent with the literature.[20,28,29] In the various protocols used in this study, the bone surface and salivary glands received the highest absorbed doses, and this finding also is in agreement with reports from previous studies.[13,14,20,30] The bone surface shows high absorbed dose values because of the great attenuation of x-rays by bone. The location of the salivary gland tissues—in the center of rotation during x-ray beam and detector movement for both panoramic and CBCT examinations—explains the high absorbed dose of this organ. Even if most of the scanned

anatomy is only momentarily irradiated, structures at the rotational centers are exposed longer or continuously.

An interesting finding in this study was that between the adult and child phantoms, the radiation burden was significantly larger with the Veraviewepocs 3-D F40 unit than with the Veraview X800 unit when used with the manufacturer's default settings for the supposed patient ages of the phantoms. We believe that the more compact design of the Veraviewepocs 3-D F40 unit with an x-ray focal spot−center of rotation distance of 340 mm, versus 400 mm for the Veraview X800 unit, was the reason for the larger difference in radiation burden. For the same dose at the surface of the detector, the effect of the inverse square law will be more pronounced when the distance to the x-ray focal spot is 14% to 36% less, resulting in higher doses and greater radiation burden.

Differences in the locations and sizes of the organs could also contribute to differences between the phantoms. Wahid et al.[31] and Al Najjar et al.[32] reported ambiguous results when comparing absorbed doses to organs and tissues in adult and child phantoms; that is, they found both higher and lower doses for adults compared with children. Moreover, Choi and Ford[33] reported higher absorbed doses for a child phantom compared with the adult with use of an ionization chamber.

The depth dose characteristics for the TMJ protocols depend on (1) the attenuation of the primary beam (in its dependence on kilovoltage and filtration); (2) the focal spot−isocenter distance (inverse square law); and (3) the buildup of scatter radiation. The 3 units studied were indeed very different with regard to these parameters, as summarized in Table II.

The greater decrease in depth dose as a result of the shorter isocenter distance for the Veraviewepocs 3-D F40 and Veraview X800 units than for the 3-D Accuitomo 170 unit is compensated for by the much higher filtration, making the primary attenuation lower; the extent of this effect could be studied by using measurements in a homogeneous water phantom.

Because of these construction differences, it is not evident whether the doses to the child phantom, in general, should be larger than those to the adult phantom. For instance, as can be seen in Table VI, the mean dose to the brain is higher for the adult, probably because the adult phantom is larger and the distance from the x-ray source to the entrance point of the phantom, especially at the back of the head, is approximately 20 mm shorter than for the child phantom, resulting in a higher entrance dose.

The smaller dimensions of the child phantom can affect the dosage compared with those of the adult phantom for other reasons. For instance, the eye dose for a full rotation was significantly higher for the child phantom (see Table IV); this is because the eye of the child is closer to the irradiated 4 × 4 cm volume.

The 3-D Accuitomo 170 unit has an even longer distance (540 mm) between the x-ray source and the center of rotation. Accordingly, the radiation burden was highest for the Veraviewepocs 3-D F40 unit, followed by the Veraview X800 unit; the 3-D Accuitomo 170 unit had the lowest radiation burden (see Table V). A notable finding was that organ doses generally were not halved when using the half-rotation protocol instead of the full-rotation protocol. The reason is the position of the organs, for example, the eyes, in relation to the start and stop angles of a half rotation.

As an independent method for comparison, we used the PCXMC Monte Carlo program[34] to verify some of our measurements. To calculate the doses for the rotational geometry of the CBCT units, we used the PCXMC20 Rotation module supplied with the program. Focal spot−isocenter distance, field size, kilovoltage, and measured filtration values were entered for the dose calculations. The measured kilovoltage, filtration, and output of the x-rays impinging on the phantom were almost unaffected by position over the 4 × 4 cm radiation field. We used the mean dose to the salivary glands for the comparison (see Table IV). For the 3-D Accuitomo 170 unit, the measured mean dose for the child was 12% higher than that for the adult. The Monte Carlo calculations resulted in a 9% higher dose for the child. For the Veraview X800 unit, the corresponding numbers were 13% lower (measured) and 10% lower (calculated) for the child compared with the adult.

Our results clearly indicate that with the same exposure parameters, the use of 2 separate small FOVs (1 for each TMJ) generally results in lower doses and radiation burden compared with 1 large FOV that captures both TMJs simultaneously. Furthermore, a smaller voxel size associated with the smaller FOV could lead to better image quality. Nascimento et al.[13] reported a similar reduction in radiation burden. Lukat et al.[16] found similar results, although they compared different units.

In this study, we used 2 different phantoms that were available in our institution. Dosimetric methods that can be used in the present situation are those based on TLDs, optically stimulated luminescence dosimeters, or self-developing films, such as the Gafchromic film. However, use of LiF or aluminum oxide dosimeters in a soft tissue environment will create a problem because these dosimeters have a pronounced energy dependence in a 30−150 kiloelectron-volt interval because of their higher atomic number.[35,36] Because the x-ray spectrum varies with the position in the phantom, the actual absorbed doses in the phantom where such dosimeters were placed would be very difficult to estimate. Hourdakis and Nowotny[37] expressed their concerns about the use of LiF and aluminum oxide dosimeters in radiation fields with spatially varying x-ray spectra.

The radiosensitive material in the Gafchromic film is diacetylene. The mass−energy absorption coefficient, μ_{en}/ρ, calculated by using National Institute of Standards and Technology data[38] for this material, has an energy dependence perfectly parallel to that of water (soft tissue), making it suitable as a dosimeter because it has the same energy absorption characteristics as its surrounding material. Compared with air, the μ_{en}/ρ characteristics coincide, which explains why the calibration curves for different kilovolt values are the same. This notion was supported by Hourdakis and Nowotny.[37] The high spatial resolution of the film is another desirable property for mapping dose distributions in radiation fields with steep dose gradients, as is the case in dental radiology. Placing a TLD ± 3 mm from a point in the gradient can result in up to 85% variation in the measured signal from the dosimeter. Indeed, most of the radiation dosimeters are limited in that the organ dose depends on loading the dosimeters in manufacturer-determined locations in the phantom as a representative of the whole organ volume.

For the Gafchromic film, using the red channel of the RGB 24-bit images will give a more sensitive system (a steeper calibration curve). This also means that a small variation in pixel values in the high end of the usable interval will give a large increase in absorbed dose. We preferred to extend the dose measurement range instead by converting the RGB image to an 8-bit gray scale. Moreover, use of multiple color channels to convert the scanned images on the Gafchromic film into dose maps compensates for many of the common disturbances that are usually associated with this dosimetric method, such as the nonuniform thickness of the film's active layer, thus adding to data integrity and dosimetric accuracy.[39]

The currently available x-ray units with their different settings are usually associated with varying amounts of radiation. Because of the differences in their construction, it is important to make the dose measurements specific to each unit to estimate patient radiation doses. Therefore, interpretation and comparison of dosimetric studies must be made with caution.

Weighing the risks and benefits of exposure to ionizing radiation is a vital matter to be considered carefully, particularly for children, as their developing tissues are more radiosensitive than adult tissues and their longer life expectancy increases the lifetime risk for developing radiation-induced cancers. Furthermore, selection of the proper radiographic examinations with the most appropriate clinical setting, as well as use of low dose protocols, is important to ensure diagnostic accuracy while adhering to the ALADA[2] principle.

CONCLUSIONS

The absorbed doses within and between radiosensitive organs and tissues varied widely. Mean absorbed dose to the brain, eyes, salivary glands, oral mucosa, and bone surface varied considerably between adult and child phantoms. The bone surface and the salivary glands received the highest absorbed doses compared with other tissues, both in panoramic radiography and CBCT of the TMJ. The radiation burden to the adult phantom was generally higher than for the child phantom. The mean doses measured were smaller when using 2 (bilateral) 4 × 4 cm volumes than for one 14 × 5 cm volume.

DISCLOSURE

The authors declare no conflicts of interest.

FUNDING

This study was funded by King Abdulaziz University.

ACKNOWLEDGMENT

We are grateful to radiographer Curt Johansson for his help during the practical part of this study.

REFERENCES

1. Demeter S, Applegate KE, Perez M. Internet-based ICRP resource for healthcare providers on the risks and benefits of medical imaging that uses ionising radiation. *Ann ICRP*. 2016;45:148-155.
2. Bushberg JT. Science, radiation protection, and the NCRP: building on the past, looking to the future. In: Proceedings of the fiftieth annual meeting program of NCRP: achievements of the past 50 years and addressing the needs of the future, March 10-11; 2014. Bethesda, MD. pp. 5-7.
3. Lewis EL, Dolwick MF, Abramowicz S, Reeder SL. Contemporary imaging of the temporomandibular joint. *Dent Clin North Am*. 2008;52:875-890.
4. Ahmad M, Hollender L, Anderson Q, et al. Research diagnostic criteria for temporomandibular disorders (RDC/TMD): development of image analysis criteria and examiner reliability for image analysis. *Oral Surg Oral Med Oral Pathol Oral Radiol Endod*. 2009;107:844-860.
5. Schmitter M, Gabbert O, Ohlmann B, et al. Assessment of the reliability and validity of panoramic imaging for assessment of mandibular condyle morphology using both MRI and clinical examination as the gold standard. *Oral Surg Oral Med Oral Pathol Oral Radiol Endod*. 2006;102:220-224.
6. Zain-Alabdeen EH, Alsadhan RI. A comparative study of accuracy of detection of surface osseous changes in the temporomandibular joint using multidetector CT and cone beam CT. *Dentomaxillofac Radiol*. 2012;41:185-191.
7. Honda K, Larheim TA, Maruhashi K, Matsumoto K, Iwai K. Osseous abnormalities of the mandibular condyle: diagnostic reliability of cone beam computed tomography compared with helical computed tomography based on an autopsy material. *Dentomaxillofac Radiol*. 2006;35:152-157.
8. Tsiklakis K, Syriopoulos K, Stamatakis HC. Radiographic examination of the temporomandibular joint using cone beam computed tomography. *Dentomaxillofac Radiol*. 2004;33:196-201.
9. Devic S. Radiochromic film dosimetry: past, present, and future. *Phys Med*. 2011;27:122-134.
10. Butson MJ, Yu PKN, Cheung T, Alnawaf H. Energy response of the new EBT2 radiochromic film to x-ray radiation. *Radiat Meas*. 2010;45:836-839.

11. Hellen-Halme K, Nilsson M. The effects on absorbed dose distribution in intraoral x-ray imaging when using tube voltages of 60 and 70 kV for bitewing imaging. *J Oral Maxillofac Res*. 2013;4:e2.
12. Watanabe Y, Patel G, Patel P. Evaluation of a new self-developing instant film for imaging and dosimetry. *Radiat Prot Dosimetry*. 2006;120:121-124.
13. Nascimento HAR, Andrade MEA, Frazão MAG, Nascimento EHL, Ramos-Perez FMM, Freitas DQ. Dosimetry in CBCT with different protocols: emphasis on small FOVs including exams for TMJ. *Braz Dent J*. 2017;28:511-516.
14. Kadesjö N, Benchimol D, Falahat B, Näsström K, Shi X. Evaluation of the effective dose of cone beam CT and multislice CT for temporomandibular joint examinations at optimized exposure levels. *Dentomaxillofac Radiol*. 2015;44:20150041.
15. Oliveira MVL, Andrade MEA, Batista WO, Campos PSF. Skin doses on the lens for temporomandibular joint exam in cone beam computed tomography. *Braz Arch Biol Technol*. 2015;58:886-890.
16. Lukat T, Wong J, Lam E. Small field of view cone beam CT temporomandibular joint imaging dosimetry. *Dentomaxillofac Radiol*. 2013;42:20130082.
17. Librizzi ZT, Tadinada AS, Valiyaparambil JV, Lurie AG, Mallya SM. Cone-beam computed tomography to detect erosions of the temporomandibular joint: effect of field of view and voxel size on diagnostic efficacy and effective dose. *Am J Orthod Dentofacial Orthop*. 2011;140:e25-e30.
18. Ptaszkiewicz M, Braurer-Kirsch E, Klosowski M, Czopyk L, Olko P. TLD dosimetry for microbeam radiation therapy at the European Synchrotron Radiation Facility. *Radiat Meas*. 2008;43:990-993.
19. Rampado O, Bianchi SD, Cornetto AP, Rossetti V, Ropolo R. Radiochromic films for dental CT dosimetry: a feasibility study. *Phys Med*. 2014;30:18-24.
20. Al-Okshi A, Nilsson M, Petersson A, Wiese M, Lindh C. Using GafChromic film to estimate the effective dose from dental cone beam CT and panoramic radiography. *Dentomaxillofac Radiol*. 2013;42:20120343.
21. Möller T, Reif E. *Cross-Sectional Anatomy. Pocket Atlas. CT and MRI. Volume1: Head, Neck, Spine, and Joints*. New York: Thieme Medical Publishers; 1994.
22. Burlin TE. Cavity chamber theory. In: Attix FH, Roesch WC, eds. *Radiation Dosimetry. Volume I: Fundamentals*, Cambridge, MA: Academic Press; 1968. p. 362.
23. Poludniowski G, Landry G, DeBlois F, Evans P, Verhaegen F. SpekCalc: a program to calculate photon spectra from tungsten anode x-ray tubes. *Phys Med Biol*. 2009;54:N433-N438.
24. Evans RD. X-ray and γ-ray interactions. In: Attix FH, Roesch WC, eds. *Radiation Dosimetry. Volume I: Fundamentals*, Cambridge, MA: Academic Press; 1968. p. 135.
25. Brenner DJ. Effective dose: a flawed concept that could and should be replaced. *Br J Radiol*. 2008;81:521-523.
26. Brenner DJ. We can do better than effective dose for estimating or comparing low-dose radiation risks. *Ann ICRP*. 2012;41:124-128.
27. McCollough CH, Christner JA, Kofler JM. How effective is effective dose as a predictor of radiation risk? *AJR Am J Roentgenol*. 2010;194:890-896.
28. Grünheid T, Schieck JRK, Pliska BT, Ahmad M, Larson BE. Dosimetry of a cone-beam computed tomography machine compared with a digital x-ray machine in orthodontic imaging. *Am J Orthod Dentofacial Orthop*. 2012;141:436-443.
29. Ludlow JB, Davies-Ludlow L, Brooks S, Howerton W. Dosimetry of 3 CBCT devices for oral and maxillofacial radiology: CB Mercuray, NewTom 3 G and i-CAT. *Dentomaxillofac Radiol*. 2006;35:219-226.
30. Ludlow JB, Davies-Ludlow LE, White SC. Patient risk related to common dental radiographic examinations: the impact of 2007 International Commission on Radiological Protection recommendations regarding dose calculation. *J Am Dent Assoc*. 2008;139:1237-1243.
31. Wahid MA, Choi E, MacDonald DS, Ford NL. Dosimetry analysis of panoramic−imaging devices in different−sized phantoms. *J Appl Clin Med Phys*. 2017;18:197-205.
32. Al Najjar A, Colosi D, Dauer LT, et al. Comparison of adult and child radiation equivalent doses from 2 dental cone-beam computed tomography units. *Am J Orthod Dentofacial Orthop*. 2013;143:784-792.
33. Choi E, Ford NL. Measuring absorbed dose for i-CAT CBCT examinations in child, adolescent and adult phantoms. *Dentomaxillofac Radiol*. 2015;44:20150018.
34. Tapiovaara M, Siiskonen T. *PCXMC: A Monte Carlo Program for Calculating Patient Doses in Medical X-ray Examinations*. 2nd ed. Helsinki, Finland: Radiation and Nuclear Safety Authority; 2008 Report STUK-A231.
35. Mobit P, Agyingi E, Sandison G. Comparison of the energy-response factor of LiF and Al_2O_3 in radiotherapy beams. *Radiat Prot Dosimetry*. 2006;119:497-499.
36. Agyingi EO, Mobit PN, Sandison GA. Energy response of an aluminium oxide detector in kilovoltage and megavoltage photon beams: an EGSnrc Monte Carlo simulation study. *Radiat Prot Dosimetry*. 2006;118:28-31.
37. Hourdakis J, Nowotny R. *Instrumentation for dosimetry*. Diagnostic Radiology Physics. A Handbook for Teachers and Students. Vienna, Austria: International Atomic Energy Agency; 2014.
38. XCOM: Photon Cross Sections Database, NIST Standard Reference Database 8 (XGAM) National Institute of Standards and Technology, U.S. Department of Commerce, Gaithersburg, MD 20899. Available at: https://www.nist.gov/pml/xcom-photon-cross-sections-database. Accessed 11 March 2019.
39. Micke A, Lewis DF, Yu X. Multichannel film dosimetry with nonuniformity correction. *Med Phys*. 2011;38:2523-2534.

Reprint requests:

Durer Iskanderani
Department of Oral and Maxillofacial Radiology
Faculty of Odontology
Malmö University
SE-205 06 Malmö
Sweden.
Durer.iskanderani@mau.se